

Accepted Manuscript

Chiral manganese (IV) complexes derived from Schiff base ligands: Synthesis, characterization, in vitro cytotoxicity and DNA/BSA interaction

Zhen Li, Meiju Niu, Guoliang Chang, Changqiu Zhao

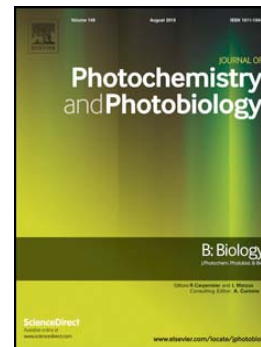
PII: S1011-1344(15)00370-X
DOI: doi: [10.1016/j.jphotobiol.2015.11.005](https://doi.org/10.1016/j.jphotobiol.2015.11.005)
Reference: JPB 10192

To appear in:

Received date: 3 August 2015
Revised date: 5 November 2015
Accepted date: 6 November 2015

Please cite this article as: Zhen Li, Meiju Niu, Guoliang Chang, Changqiu Zhao, Chiral manganese (IV) complexes derived from Schiff base ligands: Synthesis, characterization, in vitro cytotoxicity and DNA/BSA interaction, (2015), doi: [10.1016/j.jphotobiol.2015.11.005](https://doi.org/10.1016/j.jphotobiol.2015.11.005)

This is a PDF file of an unedited manuscript that has been accepted for publication. As a service to our customers we are providing this early version of the manuscript. The manuscript will undergo copyediting, typesetting, and review of the resulting proof before it is published in its final form. Please note that during the production process errors may be discovered which could affect the content, and all legal disclaimers that apply to the journal pertain.



Chiral manganese (IV) complexes derived from Schiff base ligands: synthesis, characterization, in vitro cytotoxicity and DNA/BSA interaction

Zhen Li, Meiju Niu*, Guoliang Chang, Changqiu Zhao.

Shandong Provincial Key Laboratory of Chemical Energy Storage and Novel Cell Technology, College of Chemistry and Chemical Engineering, Liaocheng University, Liaocheng, Shandong 252059, China

ABSTRACT

Two new couples of chiral manganese (IV) complexes with Schiff-base ligands, Δ -[Mn(R-L¹)₂] \cdot 2(CH₃OH) (**A-1**) and Δ -[Mn(S-L¹)₂] \cdot 2(CH₃OH) (**A-1**), Δ -[Mn(R-L²)₂] \cdot (H₂O)₂ (**A-2**) and Δ -[Mn(S-L²)₂] \cdot (H₂O)₂ (**A-2**), {H₂L¹ = (R/S)-(±)-1-[(1-hydroxymethyl-propylimino)-methyl]-naphthalen-2-ol, H₂L² = (R/S)-(±)-1-[(1-Hydroxymethyl-2-phenyl-ethylimino)-methyl]-naphthalen-2-ol} have been synthesized, and fully characterized by elemental analyses, UV-Vis spectrum, circular dichroism spectrum, FT-IR spectrum, mass spectrum, single crystal X-ray diffraction (SXRD). The interaction of the four chiral Mn (IV) complexes with CT-DNA and BSA were also investigated by various spectroscopic techniques (UV-visible, fluorescence spectroscopic). The results show that the Δ -complexes exhibit more efficient CT-DNA interaction with respect to the Λ -complexes. All the complexes could quench the intrinsic fluorescence of BSA by a static quenching process. In addition, the vitro cytotoxicity of these complexes toward four kinds of cancerous cell lines (A549, HeLa, HL-60, and Caco-2) was assayed by the MTT method, which exhibited to be selectively active against certain cell lines.

Keywords: Chiral Schiff-base; Manganese complexes; DNA binding; BSA interaction; Cytotoxicity.

1. Introduction

* Corresponding author  Tel: +86 0635 8230665; Fax: +86 0635 8239121.

E-mail address: niumeiju@163.com.

Nowadays, the cancer is the most of intractable disease, the morbidity and mortality of which have been increased [1]. Trávníček et al. have synthesized the transition metal complexes, which show highly cytotoxic [2]. Niu and coworkers have successfully prepared manganese complexes that exhibit great anticancer activities. Moreover, as one of the most primary bio-metals, manganese has become the subject of fairly extensive research for the past couple of decades [3], especially higher valent manganese. Manganese-containing compounds with pharmacological use include the anticancer agent SC-52608 and the MRI contrast agent Teslascan [4]. Chiral Schiff-base metal complexes have attracted much more attention because of its biological and pharmacy importance [5–8]. Specially, the manganese complexes are of considerable interests due to their important applications in the probe of chiral structures for biological systems, the preparation of chiral catalysts and the development of multifunctional materials [9, 10]. Moreover, it is generally counted that chiral manganese complexes are less environmentally damaging than other transition metal complexes [11]. However, until now, the reports for chiral amino alcohols Schiff-base manganese (IV) complexes are relatively rare. Therefore, the investigations on the synthesis, optical properties and biological activity of chiral amino alcohols Schiff-base metal complexes are of paramount importance [12–14].

Very recently, we have reported the synthesis, structure and biological activity of the non-chiral transition metal complexes and dealt with seeking for low toxicity, high efficiency of anticancer drugs and specific DNA target interaction [15–17]. Herein, we reported the synthesis and characterization of H_2L^1 , H_2L^2 and their manganese complexes: **A-1** (1), **A-1** (2), **A-2** (3) and **A-2** (4). The conclusion reveals that chiral complexes interactions to DNA/BSA are more strongly than that of non-chiral complexes. In addition, these complexes appeared to be selectively active and IC_{50} values of them are smaller than that of the previous non-chiral complexes.

2 Experimental

2.1 Materials and Physical measurements

All solvents and reagents were purchased commercially available and used without further purification. The two ligands, H_2L^1 , H_2L^2 had been synthesized in our laboratory. IR spectra were recorded on Nicolet-5700 FT-IR spectrophotometer with KBr pellets in the 4000-400 cm^{-1} region. UV-Vis spectra were performed on a UV-2550 ultraviolet spectrophotometer. 1H NMR spectra were obtained on a Varian Mercury Plus 400 MHz NMR spectrometer. Elemental analyses for C, H and N were performed at a PE-2400-II apparatus. Electrospray ionization mass spectroscopic (ESI-MS) analyses are performed with a Bruker microTOF-Q mass spectrometer (Bruker Daltonics Inc., Billerica, MA), and the mass spectra are obtained in the positive mode. Circular dichroism (CD) spectra measurements were measured on a Jasco J-810 spectropolarimeter. Electronic absorption spectra were recorded using a HP-8453A diode array spectrophotometer. Emission spectra were measured with LS55 spectrofluorometer.

2.2 Synthesis of ligands

2.2.1 Synthesis of (*R*)- H_2L^1

The methanol solution (10 mL) of *R*-(-)-2-amino-1-butanol (0.446 g, 5 mmol) were added to the methanol solution (10 mL) of 2-hydroxy-1-naphthaldehyde (0.861 g, 5 mmol), respectively. The mixture was refluxed for 4 h under the magnetic stirring and the resultant yellow solution was evaporated to dryness using rotavapor and vacuum pump. A schematic representation of ligand synthesis is given in Scheme 1. Then the resulting yellow precipitate or oily liquids was dried in vacuum to give (*R*)-/(*S*)- H_2L . The synthetic procedures for other ligands were very similar as the (*R*)- H_2L^1 and discussed together in follow.

(*R*)- H_2L^1 Yield: 89.0%; M.p.: 171–173°C; *Anal.* Calc. (%) for $C_{15}H_{17}NO_2$ ($M_r = 243.30$): C, 74.05; H, 7.04; N, 5.76%. Found: C, 73.98; H, 6.98; N, 5.75%. Selected IR (KBr pellet: cm^{-1}): 3446 (s, ν_{O-H}), 1625 (s, $\nu_{C=N}$), 1100 (s, ν_{Ar-O}). 1H NMR (400 MHz, $CDCl_3$) δ/ppm 8.62 (s, 1H, $-CH=N$), 7.69–6.62 (m, 6H, Ar-**H**), 3.84 (m, 1H, **CH**), 3.70 (m, 2H, $-CH_2OH$), 1.64 (m, 2H, $-CH_2CH_3$), 1.01 (t, 3H, $-CH_2-CH_3$).

(*R*)-H₂L² Yield: 86.2%; M.p.: 181–183 °C; *Anal.* Calc. (%) for C₂₀H₁₉NO₂ (Mr = 305.37): C, 78.66; H, 6.27; N, 4.59%. Found: C, 78.05; H, 6.54; N, 4.32%. Selected IR (KBr pellet: cm⁻¹): 3442 (s, ν_{O-H}), 1620 (s, ν_{C=N}), 1107 (s, ν_{Ar-O}). ¹H NMR (400 MHz, CDCl₃) δ/ppm 8.41 (s, 1H, –CH=N), 7.52–6.68 (m, 11H, Ar–H), 3.91 (m, 1H, CH), 3.71 (m, 2H, –CH₂OH), 3.01–2.92 (m, 2H, Ph–CH₂–).

2.3 Syntheses of complexes 1–4

Four manganese (IV) complexes **1–4**, reported here, were prepared according to the following general procedure. The methanol solution of the respective chiral ligand (0.4 mmol) was added to Mn(OAc)₂·4H₂O (0.0490 g, 0.2 mmol). The mixture was allowed to be stirred at room temperature for 5 h and then filtered. The dark brown crystals suitable for X-ray data collection were obtained by slow evaporation of methanol solution for two week.

A-[Mn(R-L¹)₂]·**2(CH₃OH) (1)** Yield: 79.8%. M.p.: 167–168 °C. *Anal.* Calc. (%) for C₃₂H₃₈MnN₂O₆ (Mr = 601.58): C, 63.89; H, 6.37; N, 4.66 %. Found: C, 63.83; H, 6.32; N, 4.65 %. Selected IR (KBr pellet: cm⁻¹): 1616 (s, ν_{C=N}), 1093 (s, ν_{Ar-O}), 549 (m, ν_{Mn-O}), 412 (m, ν_{Mn-N}). ESI-MS, *m/z*: 328.33 [L¹+Mn+CH₃OH+H]⁺, 592.42 [2L¹+2Mn+H]⁺, 614.17 [2L¹+2Mn+Na]⁺. UV-Vis (CH₃OH), λ_{max}/nm: 246, 308nm, 394nm.

A-[Mn(S-L¹)₂]·**2(CH₃OH) (2)** Yield: 81.0%. M.p.: 167–169 °C. *Anal.* Calc. (%) for C₃₂H₃₈MnN₂O₆ (Mr = 601.58): C, 63.89; H, 6.37; N, 4.66 %. Found: C, 63.86; H, 6.35; N, 4.62 %. Selected IR (KBr pellet: cm⁻¹): 1618 (s, ν_{C=N}), 1092 (s, ν_{Ar-O}), 548 (m, ν_{Mn-O}), 419 (m, ν_{Mn-N}). ESI-MS, *m/z*: 328.33 [L¹+Mn+CH₃OH+H]⁺, 592.33 [2L¹+2Mn+H]⁺, 614.25 [2L¹+2Mn+Na]⁺. UV-Vis (CH₃OH), λ_{max}/nm: 248, 308nm, 396 nm.

A-[Mn(R-L²)₂]·**2(H₂O) (3)** Yield: 53.2%. M.p.: 179–182 °C. *Anal.* Calc. (%) for C₄₀H₃₈MnN₂O₆ (Mr = 697.66): C, 69.39; H, 5.40; N, 3.95 %. Found: C, 69.33; H, 5.35; N, 3.94 %. Selected IR (KBr pellet: cm⁻¹): 1616 (s, ν_{C=N}), 1081 (s, ν_{Ar-O}), 538 (m, ν_{Mn-O}), 424 (m, ν_{Mn-N}). ESI-MS, *m/z*: 662.58 [2L²+Mn+H]⁺, 684.50 [2L²+Mn+Na]⁺. UV-Vis (CH₃OH), λ_{max}/nm: 246, 311 nm.

4-[Mn(S-L²)₂·2(H₂O) (4) Yield: 57.7%. M.p.:178–180 °C. *Anal. Calc.* (%) for C₄₀H₃₈MnN₂O₆ (Mr = 697.66): C, 69.06; H, 5.22; N, 4.03 %. Found: C, 69.01; H, 5.19; N, 4.02 %. Selected IR (KBr pellet: cm⁻¹): 1615 (s, ν_{C=N}), 1082 (s, ν_{Ar-O}), 543 (m, ν_{Mn-O}), 426 (m, ν_{Mn-N}). ESI-MS, *m/z*: 662.50 [2L²+Mn+H]⁺, 684.50 [2L²+Mn+Na]⁺. UV-Vis (CH₃OH), λ_{max}/nm: 248, 308 nm.

2.4 Crystal Data Collection and Refinement

Diffraction data for the title complexes were obtained on a Bruker Smart 1000 CCD diffractometer (graphite monochromized Mo K α radiation, λ = 0.71073 Å) and collected by the γ -2 θ scan technique at 298 (2) K. Empirical absorption corrections were applied using the SADABS program [18]. The semiempirical absorption correction was applied to the data. The structure was solved by direct methods by SHELXS-2014 and refined against F². All non-hydrogen atoms were refined with anisotropic thermal parameters [19]. A summary of the crystallographic data and refinement parameters for the complexes are provided in Table 1. Selected bond lengths and angles are listed in Table S1.

2.5 DNA-binding studies

The concentration of DNA was determined by using UV-Vis absorbance and the molar absorption coefficient (6600 M⁻¹ cm⁻¹) at 260 nm [20]. UV-Vis absorbance was performed by varying the concentration of complex (10 μM) in 10 mM Tris-HCl/10 mM NaCl (pH = 7.4) buffer while making the CT-DNA concentrations constant from 0 to 14 μM. For the fluorescence quenching experiments, the EB solution was added to the prepared buffer solution of CT-DNA for 2 h, and then added to the solution of complex from 0 to 48 μM. All samples were excited at 258 nm, and emission spectra were recorded at 540–700 nm.

2.6 Protein binding studies

The BSA binding experiments with manganese (IV) complexes were studied from the fluorescence spectra in 10mM buffer solution recorded with an excitation at 280 nm. In the measurement of UV-Vis spectra, the concentration of BSA was kept at 1.0×10⁻⁴ M and the complex was kept at 2.0×10⁻³ M. The fluorescence spectra were

measured at a scanning speed of 200 nm/min and slit width of 7 nm both the excitation and emission monochromators. For synchronous fluorescence spectra, we also used the same concentration of BSA and the complexes, and measured the spectra at two different $\Delta \lambda$ values, but between the excitation and emission wavelengths of BSA are different, such as 15 and 60 nm.

2.7 Cytotoxicity

In vitro cell culture studies are valuable tools for the screening of chemotherapy agents and provide preliminary data for further relative studies. The cytotoxicity of the complexes to cells was evaluated through the loss of cell viability using MTT assay [21]. Cell lines of HL-60 were grown in RPMI-1640 medium and A549, Caco-2, HeLa were grown in RPMI-DMEM medium, maintain culture at 37°C, 5% CO₂ and 95% air in the CO₂ incubator for 24h. Various concentrations of prepared complexes were added to the cells and incubation continued for 48h. Then the MTT was dissolved in medium and added to each well, and incubated for another 4h. The purple formazan crystals were solubilized by the addition of 100 μ L DMSO. The absorbance was measured at 570 nm by the ELISA reader. The values are the averages from at least three independent experiments, which were measured as the percentage ratio of the absorbance of the treated cells to the untreated controls. The IC₅₀ values were determined by the plot of percentage of cell inhibition versus concentration by non-linear regression analysis.

3 Results and discussion

3.1 IR spectrum

The IR spectra of complexes show a strong band at 1616-1618 cm⁻¹ assigned to the $\nu(\text{C}=\text{N})$ vibration, as compared to the spectra of the Schiff base ligand $\nu(\text{C}=\text{N})$ 1623–1633 cm⁻¹, which shifts lower frequency and supports the coordination of the (C=N) group [22]. The strong absorption bands of Ar–O in the Ligand at 1100–1107 cm⁻¹ locates at lower frequency for complexes, viz. 1093 cm⁻¹ for **1**, 1092 cm⁻¹ for **2**, 1081 cm⁻¹ for **3** and **4**, respectively, it could be considered that the deprotonated

phenol O group has coordinated to the manganese ion. Additional support for the formation of the complexes were provided by the existence of medium intensity bands in the region 549–538 cm^{-1} and 412–424 cm^{-1} assigned to $\nu(\text{Mn-N})$ and $\nu(\text{Mn-O})$, respectively [23].

3.2 UV-Vis spectrum

The UV-Vis spectra of the ligands and complexes are recorded in methanol solution. The ligand **2** showed four main bands in the range 227–232 nm, 245–273 nm, 305–316 nm and 405–421 nm, respectively, which may be attributed to $\pi-\pi^*$ and $n-\pi^*$ transitions of the aromatic rings and the non-bonding electrons on N atoms of imino groups [24]. While complexes displays only three strong absorption bands at 222–238 nm, 241–273 nm and 302–335 nm as compared to the bands of the ligands. It does not exhibit d-d transition due to its completely filled d^{10} electronic configuration [25].

3.3 Mass spectrum

Electrospray mass spectra of methanol solution of **1** showed an intense peak at 328.33 corresponding to the molecular fragments $[\text{L}^1+\text{Mn}+\text{CH}_3\text{OH}+\text{H}]^+$. The structure of complex **1** decomposes in polar solvents and the complex dissociates as monomers. The complex **2** has retained its dimeric structure in MeOH. The intense peaks of complex **2** are also observed at 328.33 for the molecular fragment $[\text{L}^1+\text{Mn}+\text{CH}_3\text{OH}+\text{H}]^+$. The remaining two complexes **3** and **4** have been intense peaks at 662.58 and 662.50 for the identical molecular fragment $[2\text{L}^2+\text{Mn}+\text{H}]^+$. There is no evidence for higher nuclearity fragments in solution.

3.4 Description of the structures

Complexes **1–4** are characterized by single-crystal X-ray crystallography. Since **1** and **2**, **3** and **4** are two pair of enantiomers, they have the similar crystal structures. Only the crystal structure features of complexes **1** and **3** are described in detail here.

3.4.1 $A-[Mn(R-L^1)_2]\cdot 2(CH_3OH)$ (**1**)

Single crystals of complex **1** suitable for X-ray crystallography were grown from

methanol solutions by slow evaporation method. Molecular structure of complex **1** with the atom-numbering scheme is shown in Figure 1. Selected angles and bond lengths are list in Table S1. It crystallizes in the chiral orthorhombic $P2_12_12$ space group and each asymmetric unit contains one mononuclear neutral manganese complex and two free CH_3OH solvent molecules. In complex **1**, the coordination geometry of the Mn center is octahedral, where four oxygen atoms from the $R\text{-H}_2\text{L}^1$. Each ligand contains deprotonated phenolic and alcoholic groups along with one imine nitrogen. Two oxygen atoms from alcoholic hydroxyl group and another oxygen atom from the phenolic group are located at the basal coordination plane. The apical position is occupied by two nitrogen atoms from the imine of adjacent $R\text{-H}_2\text{L}^1$ ligand, and the Mn–O and Mn–N bond lengths are very analogous in the range of 1.846(4)–1.965(4) Å. Moreover, The four oxygen atoms occupy the equatorial plane and the axial angle N(1)–Mn(1)–N(1A) is 173.43 (17)°. The O–Mn–O and O–Mn–N angles are from 84.69 (10)° to 95.31(10)°. The Mn–O–N bond distances vary from 1.850(2) Å to 1.962(3) Å and the *trans*-angles of 172.49(11)°–174.43(17)°, indicating a marginal distortion in the geometry, are in agreement with those reported for Mn complexes [26]. The mononuclear molecular are associated into 2–D supramolecular network (Figure 2) through the C–H⋯ π interactions between carbon atom C (11) and the neighboring naphthalene ring.

3.4.2 Δ -[Mn(*S*- L^1)₂] \cdot 2(CH_3OH) (2)

Since complex **2** and **1** as a pair of enantiomers, they have the similar crystal structures (Figure 3). Therefore, the crystal structure of the complex 2 is no longer described in detail here.

3.4.3 Δ -[Mn(*R*- L^2)₂] \cdot 2(H_2O) \cdot (3)

Molecular structure of complex **3** with the atom-numbering scheme is shown in Figure 4. It crystallizes in the chiral orthorhombic $P2_12_12_1$ space group and each asymmetric unit contains one mononuclear neutral manganese molecules [27] and two water solvent molecules. In complex 3, the manganese atom is six-coordinate with an

octahedral geometry. Bond dimensions, with those of complex **3**, are also in Table S1. The two imine N(1) and N(2) atoms of the amino alcohol occupy the sites. Two oxygen atoms from alcoholic hydroxyl group and another oxygen atom from the phenolic group are located at the basal coordination plane. The naphthalene rings of two ligands kept their original configurations, exhibiting no distortions. The apical position is occupied by two nitrogen atoms from the imine of adjacent dianion of $R\text{-H}_2\text{L}^2$ ligand, and the Mn–O and Mn–N bond lengths are very analogous in the range of 1.831(4)–1.972(4) Å. Moreover, The four oxygen atoms occupy the equatorial plane and the axial angle N(1)–Mn(1)–N(2) is 173.6(3)°. The O–Mn–O and O–Mn–N angles are from 86.0(3)° to 93.0(3)°. The Mn–O–N bond distances vary from 1.831(5) Å to 1.972(7) Å and the *trans*-angles of 170.1(3)°–173.6(3)°.

In the crystal structure, there are intermolecular C–H...O hydrogen bonding interactions between complex and solvent molecules resulting in a supramolecular hydrogen bonding network.

3.4.4 Δ -[Mn(S-L²)₂] \cdot 2(H₂O) (**4**)

Since complexes **4** and **3** are a pair of enantiomers, respectively, they have the similar crystal structures. However, compound **4** contains two free water molecules and one mononuclear neutral manganese complex (Figure 5). The complex **4** is associated into 3–D supramolecular net in Figure S1.

3.5 Circular dichroism spectroscopy

The CD spectra have been utilized as a powerful tool for exploring the chiral aspect of complexes and to provide valuable information about the chiral complexes [28]. The CD spectra of complex **1**, **2**, **3** and **4** in the buffer solution are shown in Figure S2 and S3. The CD spectrum of complex **1** (**A-1**) exhibits two strong positive Cotton effect peaks at $\lambda = 293, 387$ nm, and negative dichroic signal centered at $\lambda = 216, 240, 329$ nm, while complex **2** (**A-1**) shows the Cotton effects of the opposite sign at the same wavelengths. The CD spectrum of complex **3** (**A-2**) exhibits three positive peaks at $\lambda = 211, 293, 389$ nm, and negative dichroic signal centered at $\lambda = 262, 339$ nm,

while complex **4** (**4-2**) shows the Cotton effects of the opposite sign at the same wavelengths. The above CD spectral changes preliminary study suggest that the different matching of enantiomers of the chiral complexes [29]. The absolute configuration at the metal center could be determined as **Δ** or **Λ** according to the two ligands around manganese atom on the close examination of Flack parameters.

Moreover, adding the complex **1-2** and complex **1-2** in a 2:1 ratio exhibit the peaks is doubles smaller than single complexes **1-2** or **1-2** (The complexes **1** and **2** are shown in Figure S4). And adding the complexes **1-2** and **1-2** in a 1:1 ratio exhibit little peak indicated the Cotton effect of one couple chiral complexes was likely to counteract spin (Figure 6). Investigations on the circular dichroism spectroscopy indicated that synthetic four manganese (IV) complexes are chiral compounds, and complexes **1** and **2**, **3** and **4** are enantiomers, respectively.

3.6 DNA binding studies

3.6.1 UV-Vis absorption studies

The absorption spectra of complex **2**, in presence and absence of CT-DNA are shown in Figure 7 while that of complexes **1**, **3** and **4** are presented as Figure S5, S6 and S7, respectively. In the UV spectral changes, the complex **2** exhibited the intense absorption band with maxima at 251 nm which could be attributed to intra-ligand (IL) π/π^* transitions. However, increasing concentrations of CT DNA (from 0 to 14 μM) to a fixed concentration of complex exhibited an evident hyperchromism and along with a slight red shift of 3 nm. ‘Hypochromic effect’ and ‘Hyperchromic effect’ are the spectral features of CT-DNA concerning its double helix structure. Hyperchromism results from the damage of the DNA double helix structure [30, 31]. From the absorption titration data, the intrinsic binding constant (K_b) of the metal complexes with CT-DNA was determined using the equation given as:

$$[\text{DNA}]/(\varepsilon_a - \varepsilon_f) = [\text{DNA}]/(\varepsilon_b - \varepsilon_f) + 1/K_b(\varepsilon_b - \varepsilon_f)$$

To study quantitatively, the binding ability of complexes with CT-DNA, the intrinsic binding constant K_b values determined as given in Table 2. The binding constant K_b values follows the order **1-2** > **1-1** > **1-2** > **1-1**. From the results of the

binding constants, it was derived that the Mn (IV) complexes **A-1** and **A-2** revealed a stronger binding affinity for DNA double helix which was slightly higher in magnitude than complexes **A-1** and **A-2**.

3.6.2 Fluorescence quenching studies

The emission spectra of the EB-DNA system with increasing the concentration of the Mn (IV) complex **2** is shown in Figure 8 (respective spectra of complexes **1**, **3** and **4** are presented as Figure S8, S9 and S10), and the experimental data are given in Table 2. The intensity of the spectra band obviously decreases along with the increase of concentration of the complex. The result clearly indicates that the EB molecules are displaced from their DNA binding sites which are replaced by the complexes under investigation. In addition, the experimental quenching constants and binding constants of the Mn (IV) complexes **1–4** indicated that the interaction of those with DNA should be strong binding mode [32]. The Stern–Volmer quenching constant was calculated for each metal complex using the equation given as:

$$I_0/I = 1 + K_{sq}r$$

The calculated value of K_{sq} for complex **2** is higher than rest of the complexes. Moreover, **A**-complexes showed stronger binding with DNA than their **A**-complexes in all the complexes, suggesting that the DNA which is essentially chiral in nature indeed show stereochemical preference for binding with external chiral molecules. These results are in consonance with the electronic absorption titration studies given earlier in the section.

3.7 BSA-binding studies

3.7.1 Fluorescence quenching of BSA by complexes 1–4

The fluorescence of protein is due to intrinsic characteristics of tyrosine, tryptophan residues. Fluorescence quenching refers to the decreasing of the fluorophore induced by the environmental alteration around the fluorophore, which can reveal the nature of BSA binding reaction [33]. The interaction of BSA with the complex **3** on the fluorescence emission spectrum was given in Figure 9 (for complexes **1**, **2** and **4**, see Figure S11, S12 and S13). A significant decrease of the fluorescence intensity occurs

with a red shift at 347 nm, upon the addition of the Mn (IV) complex to the solution of BSA, has been observed respectively. These results suggest the formation of complex-BSA system [34]. The fluorescence quenching is described by Stem-Volmer relation:

$$I_0/I = 1 + K_{SV} [Q]$$

The K_{SV} values obtained from the plot of $[Q]$ versus I_0/I are found to be 2.44×10^4 , 4.44×10^4 , 8.32×10^4 and $9.14 \times 10^4 \text{ M}^{-1}$ for the complexes **1**, **2**, **3** and **4**, respectively, in Table 2. If it is assumed that the binding of complexes with BSA occurs at equilibrium, the equilibrium binding constant can be analyzed according to the Scatchard equation (Figure 10):

$$\log((I_0 - I)/I) = \log K_b + n \log [Q]$$

The values of K_b and n are listed in Table 2. These values of n are approximately equal to 1, suggest that there is only one binding site for these complexes on the BSA molecule. Moreover, the results indicated that **A**-complexes interact with BSA more strongly than **A**-complexes. This result is consistent with the above CT-DNA binding studies.

3.7.2 UV-Vis absorption measurements of BSA by metal complexes

UV-Vis absorption spectra could be performed to differentiate these two quenching types, dynamic quenching and static quenching [35, 36]. The representative spectra of the BSA-metal complex **2** (Figure 11, for complexes **1**, **3** and **4**, see Figure S14, S15 and S16) displays the absorption occurs with a red shift at 278 nm. This result may suggest that there exists a static interaction between the complex and BSA due to the formation of a complex-BSA ground state system, which has been found in other reported samples. In other words, the fluorescent quenching may be ascribed to static quenching.

3.7.3 Characteristic of synchronous fluorescence spectra

In order to study the structural changes of BSA in the presence of the Mn (IV) complexes, we measured synchronous fluorescence spectra with the addition of

complexes **1–4**. If the $\Delta \lambda$ value is 15 nm, the synchronous fluorescence of BSA is characteristic of a tyrosine residue and large $\Delta \lambda$ values such as 60 nm is characteristic of tryptophan [37]. The fluorescence intensity of emission corresponding to tryptophan was reflected to decrease with a bathochromic shift of emission wavelength when increasing the concentration of the complexes. And the tyrosine fluorescence emission also showed a decrease in the intensity, but with a blue shift of emission wavelength. The spectrum of complex **2** is given in Figure 12 (for complexes **1**, **3** and **4**, see Figures S17 S18 and S19). These results indicate that the metal complexes increase the polarity around the tryptophan residues and also the hydrophobicity around the tyrosine residues is strengthened. To show that in synchronous fluorescence spectroscopy confirmed the effective binding of the complexes with the BSA.

3.8 Cytotoxicity

The inhibition effects of complexes **1**, **2**, **3** and **4** against the four cell lines at a concentration of 25.0 μM are listed in Figure 13. The IC_{50} values against four cell lines are shown in Table 3. Coordination of metal ions and optical activity were essential for cytotoxicity of novel complexes. Two pairs of free ligands of IC_{50} values were much higher than the values of corresponding complexes for the coordination of metal ions play a vital role in. The complex **2** is conspicuous in displaying the prominent cytotoxicity against the tested cell lines. While the cytotoxicity of these chiral complexes showed inconsistent with previous result about enantiomer, thus the complexes are selective towards different cancerous cells. All the above results reveal that the complex **2** is higher than others, which is consistent with the high ability of **2** to bind to DNA and causes a conformational change on DNA.

As shown in Figure 13, after the tumor cells were incubated with 25.0 μM test complexes for 48 h, each complex exhibited different inhibition effect against the four cell lines, which further showed various cytotoxicity of these chiral manganese (IV) complexes against the tested cell lines even though complexes **1** and **2**, **3** and **4** possess similar structure. Such phenomenon is difficult to explain. In fact, except for

cisplatin-derivatives, there are relatively a large number of studies mechanistic information on how metal antitumour drugs function. However, it is clear that different configuration could work through different routes that lead to different cellular responses.

4 Conclusions

The use of the chiral Schiff-base ligand with manganese salts has afforded two new couples of enantiomers chiral mononuclear complexes. Single crystal X-ray diffraction studies reveal a distorted octahedral geometry around the metal centers for all complexes. Their interactions with CT-DNA and BSA were investigated using UV-visible, fluorescence and synchronous fluorescence spectroscopic methods. The results show that all complexes could quench the intrinsic fluorescence of BSA in a static quenching process, and the Δ absolute configuration of the Mn complexes exhibited more efficient DNA interaction with respect to the Λ . The vitro cytotoxic effect of the four complexes on selected cancerous cell lines exhibited substantial cytotoxic activity. Also, chiral Mn complexes are more potent than previous researched non-chiral complexes.

Abbreviations

CD	Circular dichroism
ESI-MS	Electrospray ionization mass spectroscopic
CT-DNA	Calf thymus DNA
BSA	Bovine serum albumin
EB	Ethidium bromide
MTT	3-(4, 5-dimethylthiazol-2-yl)-2, 5-diphenyltetrazolium Bromide

Acknowledgment

We acknowledge the financial support of the Natural Science Foundation of Shandong Province (No. ZR2013BM017)

Appendix A. Supplementary data

CCDC No. 1033336, 1033335, 1033334 and 1033337 for complexes **1**, **2**, **3** and **4**. These data can be obtained free of charge from the Cambridge Crystallographic Data Centre via www.ccdc.cam.ac.uk/data_request/cif.

References

- [1] D. F. Zhou, Q. Y. Chen, Y. Qi, H. J. Fu, Z. Li, K. D. Zhao, J. Gao, Anticancer Activity, Attenuation on the Absorption of Calcium in Mitochondria, and Catalase Activity for Manganese Complexes of N-Substituted Di(picoyl)amine, *Inorg. Chem.* **50** (2011) 6929–6937.
- [2] J. Vančo, Z. Šindelář, Z. Dvořák, Z. Trávníček, Iron-salophen complexes involvingazole-derived ligands: A new group of compounds with high-level and broad-spectrum in vitro antitumor activity, *J. Inorg. Biochem.* **142** (2015) 92–100.
- [3] C. P. Pradeep, P. S. Zacharias, S. K. Das, Synthesis, structural characterization and properties of an optically active mononuclear Mn(IV) complex, *Polyhedron.* **24** (2005) 1410-1416.
- [4] Z. Guo, P.J. Sadler, Metals in Medicine, *Angew. Chem. Int. Ed.* **38** (1999) 1512–1531.
- [5] Z. Dezhahang, M. R. Poopari, J. Cheramy, and Y. J. Xu, Conservation of Helicity in a Chiral Pyrrol-2-yl Schiff-Base Ligand and Its Transition Metal Complexes, *Inorg. Chem.* **54** (2015) 4539–4549.
- [6] A. Stanila, A. Marcu, D. Rusu, M. Rusu, L. David, Spectroscopic studies of some copper (II) complexes with amino acids, *J. Mol. Struct.* **834** (2007) 364–368.
- [7] N. M. Hosny, M. A. Hussien, F. M. Radwan, N. Nawar, Synthesis, spectral characterization and DNA binding of Schiff-base metal complexes derived from 2-amino-3-hydroxypropanoic acid and acetylacetone, *Spectrochim. Acta A* **132** (2014) 121–129.
- [8] M. Z. Wang, Z. X. Meng, B. L. Liu, Synthesis and spectral characterization of Schiff-base complexes derived from alanine and 2-acetylpyridine with some divalent metal acetates, *J. Coord. Chem.* **60** (2007) 2755–2764.
- [9] M. N. Dehkord, A. K. Bordbar, P. Lincoln, V. Mirkhani, Spectroscopic study on

- the interaction of ct-DNA with manganese Salen complex containing triphenyl phosphonium groups, *Spectrochimica Acta Part A*. **90** (2012) 50–54.
- [10] Z. S. Bai, Z. P. Qi, Y. Lu, Q. Yuan and W. Y. Sun, Novel Inorganic–Organic Hybrid Frameworks of Manganese (II): Syntheses, Crystal Structures, and Physical Properties, *Crystal Growth Des.* **8** (2008) 1924–1931.
- [11] M. S. Chen, Y. F. Deng, C. H. Zhang, D. Z. Kuang, Hydrothermal Synthesis and Crystal Structure of a Manganese (II) Compound Bridged by 2,6-dichlorobenzoic Acid, *Chinese J. Inorg. Chem.* **24** (2008) 1519–1522.
- [12] B. S. Jayashree, M. Kaur, A. Pai, Synthesis, characterisation, antioxidant and anticancer evaluation of novel schiff's bases of 2-quinolones, *Elixir Org. Chem.* **52** (2012) 11317–11322.
- [13] A. Noureen, S. Saleem, T. Fatima, H. M. Siddiqi, B. Mirza, , *Pak J. Pharm. Sci.* **26** (2013) 113–123.
- [14] F. Arjmand, F. Sayeed, M. Muddassir, Synthesis of new chiral heterocyclic Schiff base modulated Cu (II)/Zn (II) complexes: Their comparative binding studies with CT-DNA, mononucleotides and cleavage activity, *J. Photochem. Photobio. B* **103** (2011) 166–179.
- [15] P. Li, M. J. Niu, M. Hong, S. Cheng, J. M. Dou, Effect of structure and composition of nickel(II) complexes with salicylidene Schiff base ligands on their DNA/protein interaction and cytotoxicity, *J. Inorg. Biochem.* **137** (2014) 101–108.
- [16] M. J. Niu, M. Hong, G. L. Chang, X. Li, Z. Li, A comparative study of cytotoxicity and interaction with DNA/protein of five transition metal complexes with Schiff base ligands, *J. Photochem. Photobio. B.* **148** (2015) 232–241.
- [17] M. J. Niu, H. H. Li, S. N. Wang, Z. Q. Cao, D. W. Sun and J. M. Dou, Transition Metal Complexes with the Schiff Base Ligand 1-[[2-(2-Hydroxyethylamino) ethylimino] methyl]naphthalen-2-ol, *Z. Anorg. Allg Chem.* **639** (2013) 414–423.
- [18] G. M. Sheldrick, *Program for Empirical Absorption Correction of Area Detector Data*, University Göttingen, Göttingen, Germany, 1996.
- [19] G. M. Sheldrick, *SHELXL-97 Program for Crystal Structure Refinement*, Institut

- für Anorganische Chemie, University Göttingen, Germany, 1997.
- [20] J. Marmur, A procedure for the isolation of deoxyribonucleic acid from microorganisms, *J. Mol. Biol.* **3** (1961) 208–218.
- [21] T. Mosmann, Rapid colorimetric assay for cellular growth and survival: application to proliferation and cytotoxicity assays, *J. Immunol., Methods*, **65** (1983) 55–63.
- [22] Y. Yahsi, H. Kara, Synthesis and characterization of monomeric Mn (IV) and pseudo-tetrameric Mn (III) complexes: Magnetic properties of Mn (III) complex, *Spectrochim. Acta Part A*. **127** (2014) 25–31.
- [23] M. Belicchi-Ferrari, F. Bisceglie, G. Pelosi, P. Tarasconi, Heterocyclic substituted thiosemicarbazones and their Cu (II) complexes: synthesis, characterization and studies of substituent effects on coordination and DNA binding, *Polyhedron* **27** (2008) 1361–1367.
- [24] T. Tuerk, U. Resch, M. A. Fox, A. Vogler, Spectroscopic studies of zinc benzenethiolate complexes: electron transfer to methyl viologen, *Inorg. Chem.* **31** (1992) 1854–1857.
- [25] M. S. Nair, D. Arish, R. S. Joseyphus, Synthesis, characterization, antifungal, antibacterial and DNA cleavage studies of some heterocyclic Schiff base metal complexes, *Journal of Saudi Chemical Society* **16** (2012) 83–88.
- [26] H. Asada, M. Ozeki, M. Fujiwara, T. Matsushita, Structures of four types of novel high-valent manganese complexes obtained by the reactions of KMnO_4 with tridentate Schiff base ligands, *Polyhedron* **21** (2002) 1139–1148.
- [27] C. P. Pradeep, P. S. Zacharias, S. K. Das, A chiral Mn (IV) complex and its supramolecular assembly: Synthesis, characterization and properties, *J. Chem. Sci.*, 2006, **118**, 311–317.
- [28] R. Vijayalakshmi, M. Kanthimathi, R. Parthasarathi, B. U. Nair, Interaction of chromium(III) complex of chiral binaphthyl tetradentate ligand with DNA, *Bioorg. Med. Chem.* **14** (2006) 3300–3306.
- [29] N. H. Khan, N. Pandya, M. Kumar, P. K. Bera, R. I. Kureshy, S. H. R. Abdi, H. C. Bajaj, Chiral discrimination asserted by enantiomers of Ni (II), Cu (II) and Zn (II)

- Schiff base complexes in DNA binding, antioxidant and antibacterial activities, *Org. Biomol. Chem.* **19** (2010) 4297–4307.
- [30] S. Sobha, R. Mahalakshmi, N. Raman, Studies on DNA binding behaviour of biologically active transition metal complexes of new tetradentate N₂O₂ donor Schiff bases: Inhibitory activity against bacteria, *Spectrochimica Acta Part A.* **92** (2012) 175–183.
- [31] H. Y. Liu, L. Z. Li, Q. Guo, J. F. Dong, J. H. Li, Synthesis, crystal structure, DNA- and albumin-binding properties of a chromium (III) complex with 1,10-phenanthroline and a Schiff base derived from glycine. *Trans. Met. Chem.* **38** (2013) 441–448.
- [32] J. F. Dong, L. Z. Li, D. Q. Wang, Synthesis, Characterization, DNA-binding Properties and DNA Cleavage of a New Ternary Copper(II) Complex with Mixed-ligands of Tridentate Schiff Base and 1,10-Phenanthroline, *Chin. J. Chem.* **29** (2011) 259–266.
- [33] O.K.A. Zied, O.I.K.A. Shihi, Characterization of Subdomain IIA Binding Site of Human Serum Albumin in its Native, Unfolded, and Refolded States Using Small Molecular Probes, *J. Am. Chem. Soc.* **130** (2008) 10793–10801.
- [34] D. S. Raja, G. Paramaguru, N. S. P. Bhuvanesh, J. H. Reibenspies, R. Renganathan, K. Natarajan, Effect of terminal N-substitution in 2-oxo-1,2-dihydroquinoline-3-carbaldehyde thiosemicarbazones on the mode of coordination, structure, interaction with protein, radical scavenging and cytotoxic activity of copper(II) complexes, *Dalton Trans.* **40** (2011) 4548–4559.
- [35] P. Krishnamoorthy, P. Sathyadevi, R. R. Butorac, A. H. Cowley, N. S. P. Bhuvanesh, N. Dharmaraj, Variation in the biomolecular interactions of nickel (II) hydrazone complexes upon tuning the hydrazide fragment, *Dalton Trans.* **41** (2012) 6842–6854.
- [36] M. J. Niu, Z. Li, H. H. Li, X. Li, J. M. Dou, S. N. Wang, DNA/protein interaction, cytotoxic activity and magnetic properties of amino-alcohol Schiff base derived Cu(II)/Ni(II) metal complexes: influence of the nuclearity and metal ions *RSC Adv.* **5** (2015) 37085–37095.

- [37] L. Z. Li, Q. Guo, J. F. Dong, T. Xu, J. H. Li, DNA binding, DNA cleavage and BSA interaction of a mixed-ligand copper (II) complex with taurine Schiff base and 1, 10-phenanthroline, *J. Photochem. Photobio. B.* **125** (2013) 56–62.

ACCEPTED MANUSCRIPT

Table Captions

Table 1 Crystallographic data and structure refinement parameters for Schiff base complexes **1, 2, 3** and **4**.

Table 2 Comparison of interaction study results between complexes **1–4** on CT-DNA and protein.

Table 3 IC₅₀ (μM) of all complexes against A549, HeLa, HL-60, and Caco-2 for 48 h treatment.

Table 1 Crystallographic data and structure refinement parameters for Schiff base complexes **1**, **2**, **3** and **4**.

Compounds	1	2	3	4
Formular	C ₃₂ H ₃₈ MnN ₂ O ₆	C ₃₂ H ₃₈ MnN ₂ O ₆	C ₄₀ H ₃₈ MnN ₂ O ₆	C ₄₀ H ₃₈ MnN ₂ O ₆
Crystal system	Orthorhombic	Orthorhombic	Orthorhombic	Orthorhombic
Space group	P2 ₁ 2 ₁ 2	P2 ₁ 2 ₁ 2	P2 ₁ 2 ₁ 2 ₁	P2 ₁ 2 ₁ 2 ₁
Formular weight	601.58	601.58	697.66	697.66
<i>a</i> , Å	15.4668(15)	15.3349(17)	10.2974(8)	10.3634(12)
<i>b</i> , Å	8.8333(7)	8.7392(9)	10.5687(9)	10.6264(13)
<i>c</i> , Å	10.7394(8)	10.6613(11)	33.451(2)	33.582(3)
α ,deg	90	90	90	90
β ,deg	90	90	90	90
γ ,deg	90	90	90	90
<i>V</i> , Å ³	1467.2(2)	1428.8(3)	3640.5(5)	3698.2(7)
<i>Z</i>	2	2	4	4
<i>T</i> , K	298(2)	298(2)	298(2)	298(2)
λ , Å	0.71073	0.71073	0.71073	0.71073
ρ , g·cm ⁻³	1.362	1.398	1.273	1.253
R _{int}	0.0635	0.1332	0.0696	0.0953
R ₁ [I>2 σ (I)]	0.0447	0.0865	0.0876	0.0643
R ₁ (all data)	0.0649	0.1247	0.1473	0.1489
wR ₂ [I>2 σ (I)],	0.0884	0.1922	0.2027	0.1421
wR ₂ (all data)	0.0999	0.2378	0.2277	0.1676
residual electron density	0.32/-0.46	0.52/-0.56	0.40/-0.52	0.42/-0.21
Flack	0.01(2)	0.01(7)	0.03(4)	-0.03(3)

Table 2 Comparison of interaction study results between complexes **1–4** on CT-DNA and protein.

Complex	DNA-binding		Protein-binding		
	<i>K</i> _{sq}	<i>K</i> _b (M ⁻¹)	<i>K</i> _{SV} (M ⁻¹)	<i>K</i> _b (M ⁻¹)	<i>n</i>
1	2.18	2.96×10 ⁴	2.44×10 ⁴	6.46×10 ⁷	0.87
2	4.20	4.20×10 ⁴	4.44×10 ⁴	5.48×10 ⁷	1.64
3	2.96	3.09×10 ⁴	8.32×10 ⁴	2.30×10 ⁷	1.51
4	4.07	4.43×10 ⁴	9.14×10 ⁴	4.33×10 ⁷	1.56

Table 3 IC₅₀ (μM) of all complexes against A549, HeLa, HL-60, and Caco-2 for 48 h treatment.

Complex	A549	HeLa	HL-60	Caco-2
1	24.15±1.38	14.09±1.15	13.68±1.13	17.60±1.24
2	22.07±1.34	12.04±1.21	11.16±1.06	20.07±1.30
3	44.19±1.64	15.11±1.18	13.40±1.22	25.57±1.41
4	36.96±1.57	13.91±1.14	12.09±1.08	21.06±1.32
H ₂ L ¹	>100	>100	>100	>100
H ₂ L ²	>100	>100	>100	>100
[Mn(OAc) ₂] ₂ ·4H ₂ O	>100	>100	>100	>100

Figure Captions

Scheme 1 Synthesis of chiral complexes **1–4**.

Figure 1 Molecular structures of complex **1** (Thermal ellipsoids are shown at 30% probability level. Symmetry code: $-x+2, -y+1, z$).

Figure 2 View of the 2-D supramolecular network.

Figure 3 Molecular structures of complex **2**. (Thermal ellipsoids are shown at 30% probability level. Symmetry code: $-x+2, -y+2, z$).

Figure 4 Molecular structures of complex **3**. (Thermal ellipsoids are shown at 30% probability level).

Figure 5 Molecular structures of complex **4**. (Thermal ellipsoids are shown at 30% probability level).

Figure 6 CD spectra of chiral Schiff base complexes **3** and **4**.

Figure 7 UV-Vis absorption spectra of complex **2** (10 μM) in the absence and presence of increasing amounts of DNA (0–14 μM). Arrow shows the absorbance changes upon increasing DNA concentration.

Figure 8 Effects of complex **2** on the fluorescent spectra of EB–DNA system ($\lambda_{\text{ex}} = 258 \text{ nm}$); $C_{\text{DNA}} = 20 \mu\text{M}$; $C_{\text{EB}} = 2 \mu\text{M}$. From 1 to 8 $C_{\text{VOL}} = 0–42 \mu\text{M}$ Inset: plot of I_0/I vs r ($r = C_{\text{VOL}}/C_{\text{DNA}}$) for complexes **1–4**.

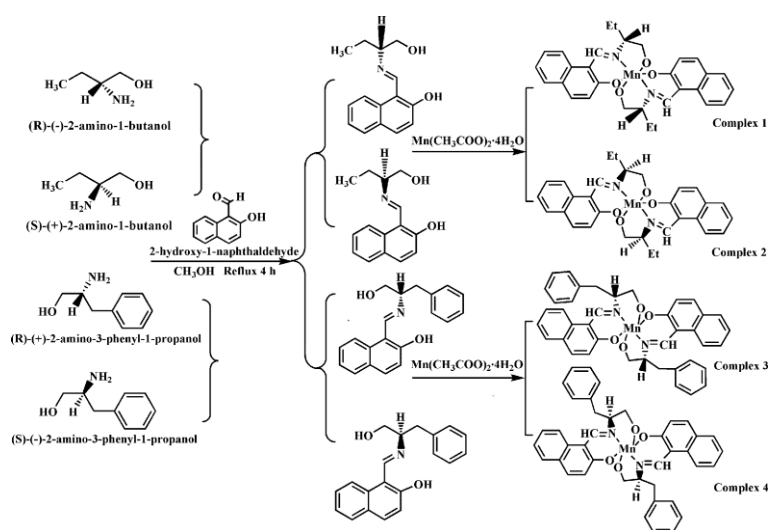
Figure 9 Emission spectra of BSA (1.0 μM ; $\lambda_{\text{ex}} = 280 \text{ nm}$) as a function of concentration of the complex **3** (0–14 μM). Arrow indicates the effect of metal complexes on the fluorescence emission of BSA.

Figure 10 Plot of $\log[(I_0-I)/I]$ vs. $\log[Q]$.

Figure 11 UV-Vis absorption spectra of BSA in the absence and presence of increasing amounts of the complex **2**. $C_{\text{BSA}} = 10 \mu\text{M}$, $[\text{Complex}] = 0$ and $10 \mu\text{M}$.

Figure 12 Synchronous spectra of BSA as a function of concentration of the complex **2** with wavelength difference of $\Delta\lambda = 15 \text{ nm}$ and $\Delta\lambda = 60 \text{ nm}$

Figure 13 Inhibition [%] of complexes **1, 2, 3** and **4** [dose level of 25.0 μM] against human tumor cells.



Scheme 1 Synthesis of chiral complexes 1–4

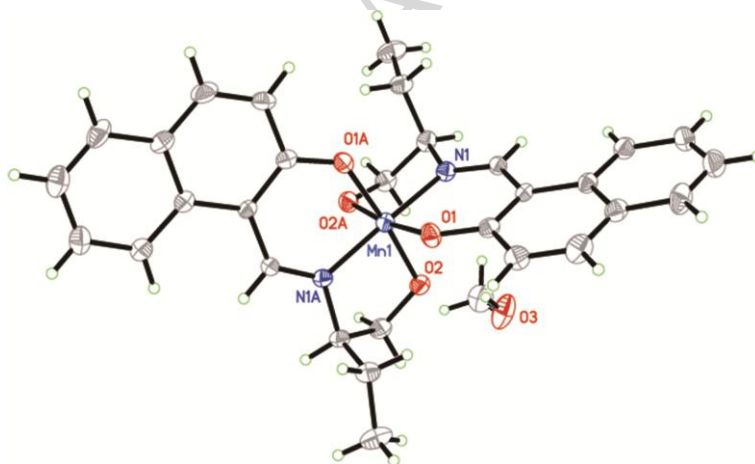


Figure 1 Molecular structures of complex 1 (Thermal ellipsoids are shown at 30% probability level. Symmetry code: $-x+2, -y+1, z$).

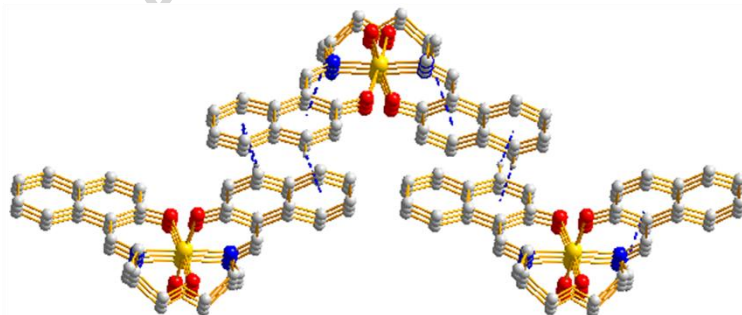


Figure 2 View of the 2-D supramolecular network.

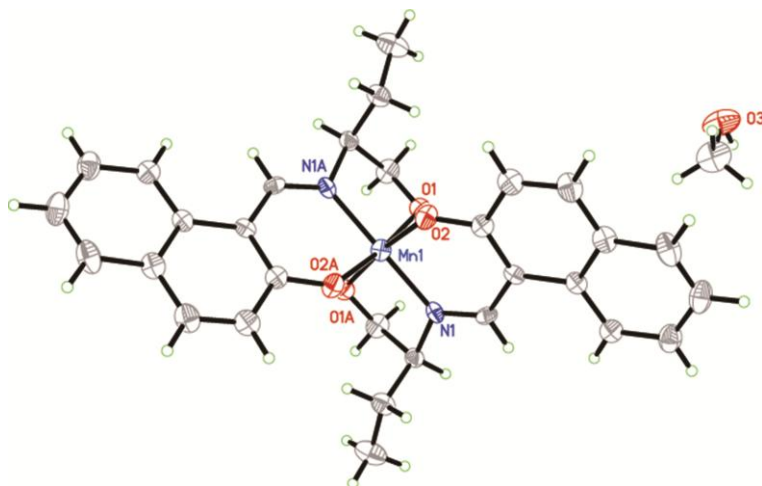


Figure 3 Molecular structures of complex 2. (Thermal ellipsoids are shown at 30% probability level. Symmetry code: $-x+2, -y+2, z$).

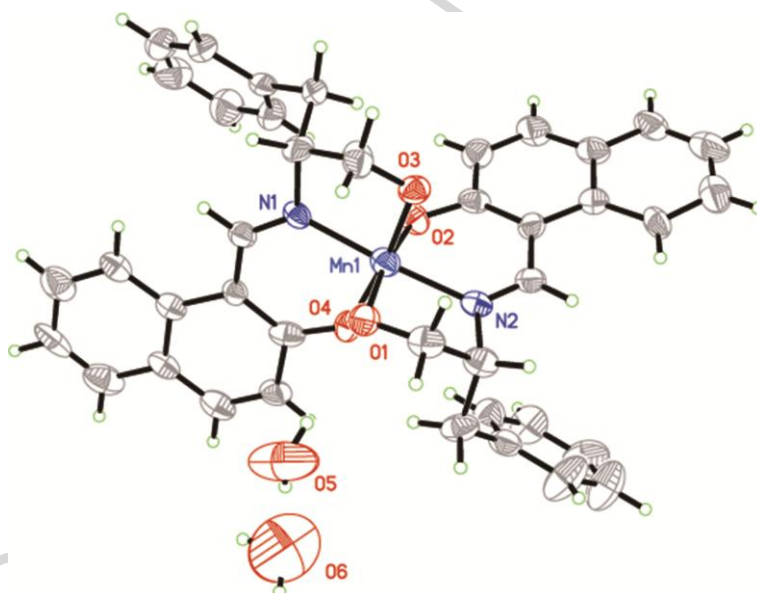


Figure 4 Molecular structures of complex 3. (Thermal ellipsoids are shown at 30% probability level).

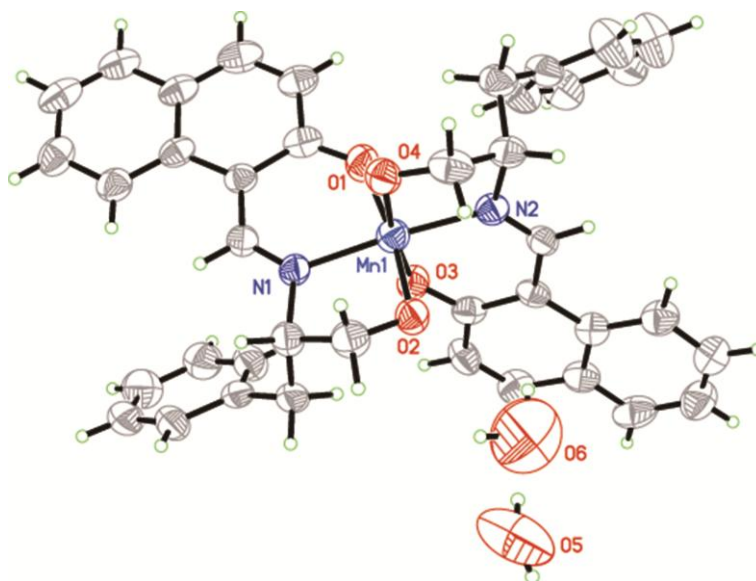


Figure 5 Molecular structures of complex 4. (Thermal ellipsoids are shown at 30% probability level).

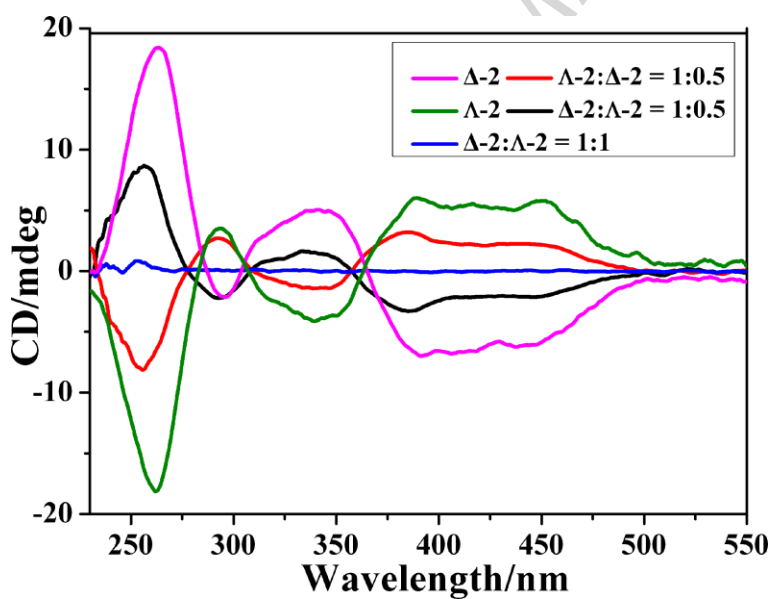


Figure 6 CD spectra of chiral Schiff base complexes 3 and 4.

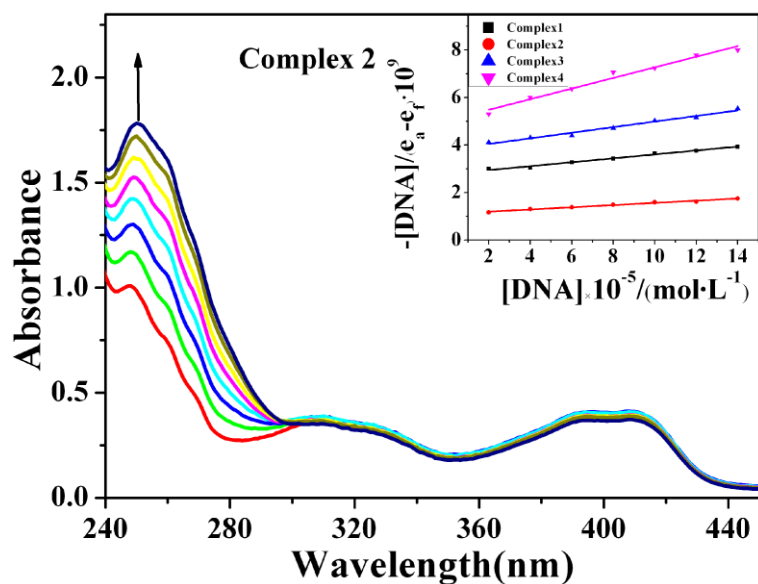


Figure 7 UV-Vis absorption spectra of complex 2 (10 μM) in the absence and presence of increasing amounts of DNA (0–14 μM). Arrow shows the absorbance changes upon increasing DNA concentration.

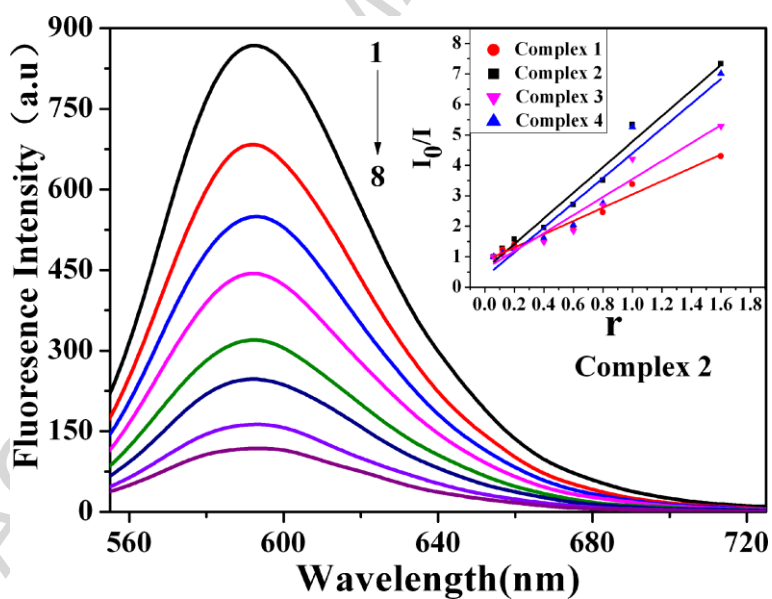


Figure 8 Effects of complex 2 on the fluorescent spectra of EB–DNA system ($\lambda_{\text{ex}}=258 \text{ nm}$); $C_{\text{DNA}}=20 \mu\text{M}$; $C_{\text{EB}}=2 \mu\text{M}$. From 1 to 8 $C_{\text{VOL}}=0-42 \mu\text{M}$ Inset: plot of I_0/I vs r ($r = C_{\text{VOL}}/C_{\text{DNA}}$) for complexes 1–4.

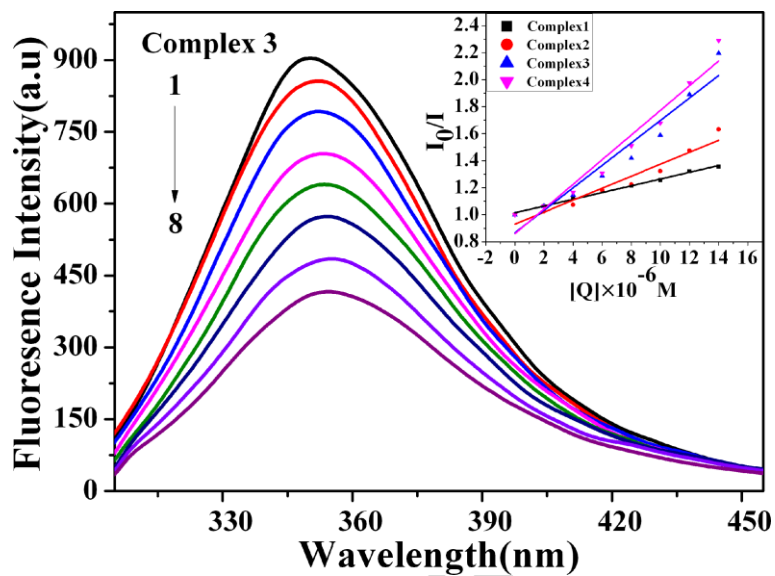


Figure 9 Emission spectra of BSA (1.0 μM; $\lambda_{ex} = 280$ nm) as a function of concentration of the complex 3 (0–14 μM). Arrow indicates the effect of metal complexes on the fluorescence emission of BSA.

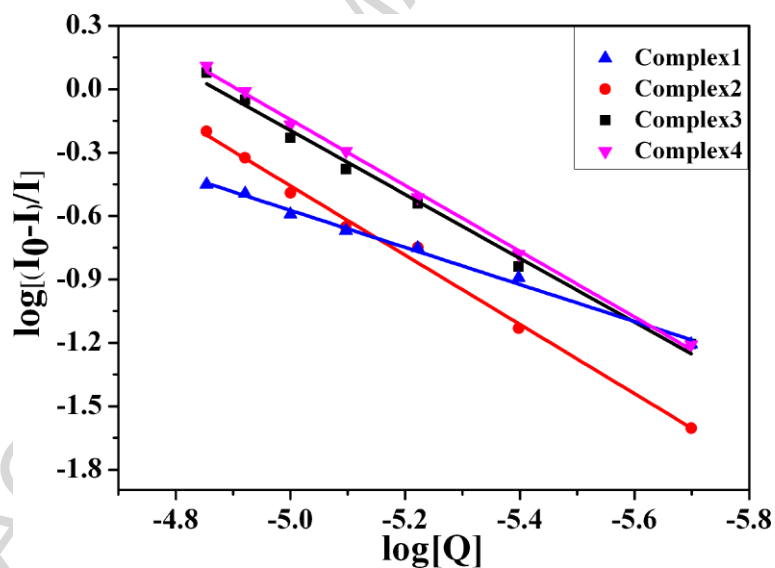


Figure 10 Plot of $\log[(I_0-I)/I]$ vs. $\log[Q]$.

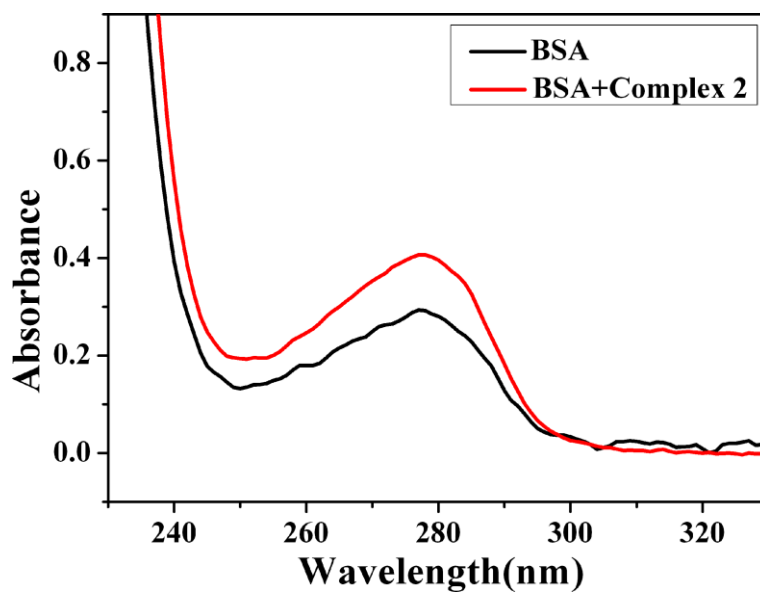


Figure 11 UV-Vis absorption spectra of BSA in the absence and presence of increasing amounts of the complex 2. $C_{BSA} = 10 \mu\text{M}$, $[\text{Complex}] = 0$ and $10 \mu\text{M}$.

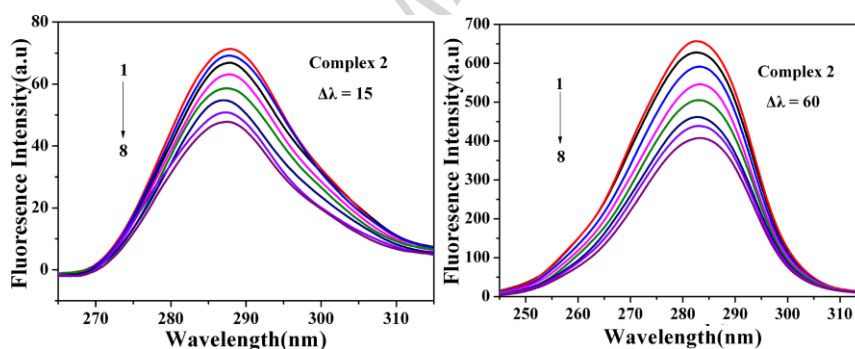


Figure 12 Synchronous spectra of BSA as a function of concentration of the complex 2 with wavelength difference of $\Delta\lambda = 15$ nm and $\Delta\lambda = 60$ nm.

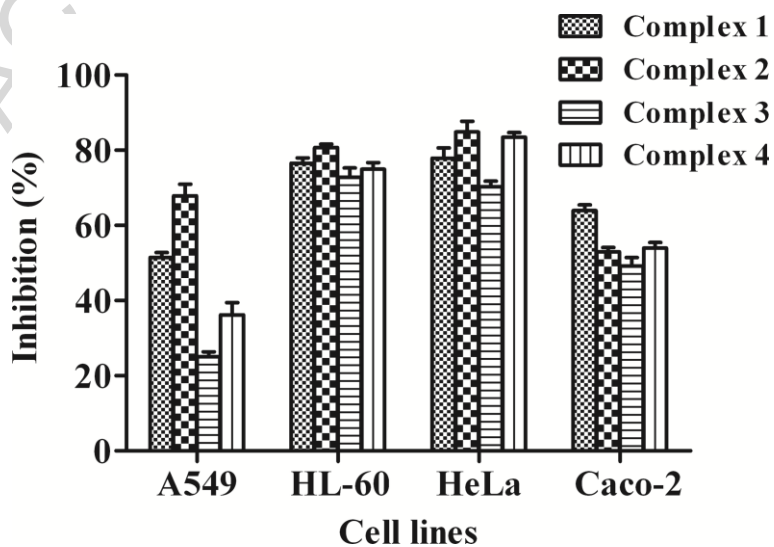


Figure 13 Inhibition [%] of complexes 1, 2, 3 and 4 [dose level of $25.0 \mu\text{M}$] against human tumor cells.

Graphical Abstract

Title	Chiral manganese (IV) complexes derived from Schiff base ligands: synthesis, characterization, in vitro cytotoxicity and DNA/BSA interaction
Authors	Zhen Li, Meiju Niu*, Guoliang Chang, Changqiu Zhao.
Affiliations	Shandong Provincial Key Laboratory of Chemical Energy Storage and Novel Cell Technology, School of Chemistry and Chemical Engineering, Liaocheng University, Liaocheng, 252059, P. R. China
Graphics	<p>The graphics section contains three main figures. At the top, four chemical structures of manganese(IV) complexes are shown, labeled Complex 1, Complex 2, Complex 3, and Complex 4. Each structure features a central Mn(IV) atom coordinated to a Schiff base ligand and two ethyl groups. Below the structures are three plots: 1) A bar chart showing the inhibition percentage of four complexes (Complex 1, 2, 3, 4) against four cell lines: A549, HL-60, HeLa, and Caco-2. 2) A UV-Vis absorption spectra plot for Complex 2, showing absorbance versus wavelength (nm) from 200 to 440 nm. 3) A fluorescence spectra plot for Complex 3, showing fluorescence intensity (a.u.) versus wavelength (nm) from 330 to 450 nm.</p>
Synopsis	Four Schiff-base manganese (IV) complexes were synthesized and characterized, which trigger significant anti-proliferative effects in cancer cell lines. Spectroscopy determination reveals that the complexes from (<i>S</i>)-Schiff base ligands show stronger DNA/BSA interaction than complexes from (<i>R</i>)-Schiff base ligands.

* Corresponding author  Tel: +86 0635 8230665; Fax: +86 0635 8239121.
E-mail address: niumeiju@163.com

Highlights

- Four chiral Schiff-base Mn (IV) complexes were synthesized and characterized.
- The interaction of the Mn (IV) complexes with CT-DNA/BSA was also investigated.
- In vitro cytotoxicity of the Mn (IV) complexes was tested by the MTT method.

ACCEPTED MANUSCRIPT